

# AMCoR

Asahikawa Medical University Repository <http://amcor.asahikawa-med.ac.jp/>

Tumor Biology (2017.6) 39(6):1010428317711311.

Ferrichrome identified from *Lactobacillus casei* ATCC334 induces apoptosis through its iron-binding site in gastric cancer cells.

Masami Ijiri, Mikihiro Fujiya, Hiroaki Konishi, Hiroki Tanaka,  
Nobuhiro Ueno, Shin Kashima, Kentaro Moriichi, Junpei  
Sasajima, Katsuya Ikuta, Toshikatsu Okumura

## Ferrichrome identified from *Lactobacillus casei* ATCC334 induces apoptosis through its iron-binding site in gastric cancer cells

Tumor Biology  
June 2017: 1–12  
© The Author(s) 2017  
Reprints and permissions:  
sagepub.co.uk/journalsPermissions.nav  
DOI: 10.1177/1010428317711311  
journals.sagepub.com/home/tub



Masami Ijiri<sup>1</sup>, Mikihiro Fujiya<sup>1</sup>, Hiroaki Konishi<sup>1</sup>, Hiroki Tanaka<sup>2</sup>,  
Nobuhiro Ueno<sup>1</sup>, Shin Kashima<sup>1</sup>, Kentaro Moriichi<sup>1</sup>, Junpei  
Sasajima<sup>1</sup>, Katsuya Ikuta<sup>1</sup> and Toshikatsu Okumura<sup>1</sup>

### Abstract

Ferrichrome is known to be a siderophore, but it was recently identified as a tumor-suppressive molecule derived from *Lactobacillus casei* ATCC334 (*L. casei*). In the present study, we investigated the effects of ferrichrome in gastric cancer cells. Cell lines and xenograft models treated with ferrichrome demonstrated growth suppression. The expression levels of cleaved poly (adenosine diphosphate-ribose) polymerase, and cleaved caspase-9 were increased by ferrichrome treatment. Although the tumor-suppressive effects of ferrichrome were almost completely diminished by the iron chelation, the reduction in the intracellular iron by ferrichrome did not correlate with its tumor-suppressive effects. An exhaustive docking simulation indicated that iron-free ferrichrome can make stable conformations with various mammalian molecules, including transporters and receptors. In conclusion, probiotic-derived ferrichrome induced apoptosis in gastric cancer cells. The iron binding site of ferrichrome is the structure responsible for its tumor suppressive function.

### Keywords

Gastric cancer, ferrichrome, anticancer, anti-tumor, siderophores, c-Jun N-terminal kinase, DNA damage-inducible transcript 3, iron chelation, probiotics, iron binding

Date received: 21 January 2017; accepted: 1 May 2017

### Introduction

Probiotics, including *Lactobacillus* and *Bifidobacterium* species, are known to bring benefit the health of their host mammals when administered in sufficient amounts.<sup>1</sup> Previous studies have revealed that probiotic bacteria are associated with various health benefits, including the conditioning of the intestinal microflora, suppression of excess allergic responses, and tumor-suppressive effects,<sup>2–4</sup> suggesting that probiotics produce anti-tumor molecules. The identification of such probiotic-derived molecules may help identify the mechanisms of probiotic tumor-suppressive effects and encourage the development of new anti-tumor drugs, but few of these tumor-suppressive molecules have actually been identified.

We have isolated several molecules, including competence and sporulation factor (CSF) and inorganic polyphosphate (poly P), from probiotic-conditioned media that

exerted protective effects against intestinal injury in a mouse model of enteritis,<sup>5–8</sup> as well as tumor-suppressive effects.<sup>9</sup> We subsequently identified the tumor-suppressive molecule ferrichrome in the conditioned media of *L. casei*.<sup>10</sup>

Ferrichrome is a siderophore, which are small, high-affinity, iron-chelating molecules derived from bacteria.<sup>11–13</sup> Our recent study revealed that ferrichrome

<sup>1</sup>Division of Gastroenterology and Hematology/Oncology, Department of Medicine, Asahikawa Medical University, Asahikawa, Japan

<sup>2</sup>Department of Legal Medicine, Asahikawa Medical University, Asahikawa, Japan

### Corresponding author:

Mikihiro Fujiya, Division of Gastroenterology and Hematology/Oncology, Department of Medicine, Asahikawa Medical University, 2-1 Midorigaoka-higashi, Asahikawa, Hokkaido 078-8510, Japan.  
Email: fujiya2008@hotmail.co.jp



activates the c-Jun N-terminal kinase (JNK)-DNA damage-inducible transcript 3 (DDIT3) pathway and upregulates the cleavage of poly(adenosine diphosphate-ribose) polymerase (PARP) in colorectal cancer cells.<sup>10</sup> A previous report showed that the endoplasmic reticulum (ER) stress response activates DDIT3 and that DDIT3-induced ER oxidase 1 $\alpha$  then activates the ER calcium-release channel IP3R1.<sup>14,15</sup> Cytoplasmic calcium then triggers the expression of JNK and Fas death receptor by activating the calcium/calmodulin-dependent protein kinase II.<sup>16,17</sup> Finally, the expression of caspases and PARP was induced.<sup>18</sup>

The suppressive effect of ferrichrome on colon cancer cells was much stronger than that of 5-fluorouracil (5-FU) or cisplatin, while the inhibitory effect against normal epithelia was less than that of other anti-tumor drugs.<sup>10</sup> However, whether or not ferrichrome has effects on other types of cancer cells, such as gastric cancer cells, and how it exerts its tumor-suppressive effect on cancer cells has been unclear.

In this study, ferrichrome exerted dosage-dependent growth inhibition effects against gastric cancer cell lines and activated apoptotic pathway, including the JNK-DDIT3 pathway. The tumor-suppressive effects of ferrichrome were diminished by the iron chelation. Although intracellular iron was reduced by ferrichrome treatment, the concentrations of iron in cancer cells were not correlated with the tumor-suppressive effects of ferrichrome. An exhaustive docking simulation indicated that iron-free ferrichrome can form stable conformations with various molecules, suggesting that iron-free ferrichrome induces apoptosis in gastric cancer cells through interactions with some tumor-associated molecules.

## Materials and methods

### Ferrichrome

Ferrichrome was purchased from Sigma-Aldrich (St. Louis, MO, USA). For iron chelation, equimolar FeCl<sub>3</sub> was added to the ferrichrome.

### Cell culture

MKN-45 and MKN-74 were provided by Japanese Collection of Research Bioresources Cell Bank. MKN-7 and NUGC-4 were supplied by Cell Resource Center for Biomedical Research, Institute of Development, and Aging and Cancer Tohoku University. All cell lines were grown in Roswell Park Memorial Institute (RPMI) 1640 supplemented with 10% (v/v) fetal bovine serum (FBS), 50 U/mL penicillin, and 50  $\mu$ g/mL streptomycin in a humidified atmosphere of 5% CO<sub>2</sub>. The cells were plated on six-well plates at a density of 10<sup>5</sup> cells/cm<sup>2</sup> and stimulated by ferrichrome diluted in high-glucose Dulbecco's Modified Eagle's Medium (DMEM).

### Cell viability

MKN-7, MKN-45, MKN-74, and NUGC-4 were used in this assay. The effects of iron-free and iron-binding ferrichrome treatment were assessed by sulforhodamine B (SRB) and 3-(4,5-dimethylthiazol-2-yl)-2,5-diphenyl tetrazolium bromide (MTT) assays. The dose of ferrichrome was 1–100  $\mu$ g/mL. These cells were seeded for 24 h before treatment and fixed every 24 h. The cell density was measured using an absorption spectrometer.

### SRB assay

The cells were seeded onto 96-well microplates at 1.0–2.0  $\times$  10<sup>4</sup> cells per well for 24 h before stimulation. The cells were fixed in 5% (w/v) trichloroacetic acid (TCA) for 1 h at 4°C and washed in distilled water (DW) four times. The microplates were then dehydrated at room temperature, stained in 0.057% SRB powder/DW (w/v), washed in 0.1% acetic acid, and re-dehydrated. The stained cells were lysed in 200  $\mu$ L per well of Tris-buffer (10 mM, pH 10.5), and the optical density (OD) was measured at 510 nm.<sup>19</sup>

### MTT assay

Cell growth was assessed using an MTT cell proliferation kit 1 (Roche Diagnostics GmbH, Mannheim, Germany). The cells were seeded onto 96-well microplates at 0.5 to 1.0  $\times$  10<sup>4</sup> per well for 24 h prior to stimulation. The cells were subsequently incubated with 10  $\mu$ L of MTT labeling reagent for 4 h, followed by addition of 100  $\mu$ L of solubilization solution into each well. The plates were left in the incubator overnight, and the OD was measured at a 570 nm test wavelength and a 650 nm reference wavelength.

### Xenograft models

The protocols of the animal experiments model were approved by the Asahikawa Medical University Institutional Care and Use Committee. BALB/c<sup>nu/nu</sup> nude mice (male, 6 weeks of age) were obtained from Sankyo Labo Service (Tokyo, Japan). About 2 h after administering anti-asialo ganglio-N-tetraosylceramide antibody, MKN-45 (1.0  $\times$  10<sup>6</sup> cells) with Matrigel was injected into the back of mice. The mice were treated with DW or 100  $\mu$ g of ferrichrome by daily intraperitoneal administration. Finally, blood cell counts of the venous blood were examined.

### Real-time polymerase chain reaction

The cells were washed with phosphate-buffered saline (PBS), and the RNA was extracted using an RNeasy Mini Kit (Qiagen, Tokyo, Japan). The messenger RNA (mRNA) of DDIT3 was reverse transcribed using a high-capacity

complementary DNA (cDNA) reverse transcription kit (Applied Biosystems, Foster City, CA, USA). The reaction was carried out at 25°C for 10 min, 37°C for 120 min, and 85°C for 5 s. The cDNA was amplified using the specific primer for DDIT3 (Applied Biosystems; Assay ID; Hs 00358796), and the gene expression signal was detected in duplicate using an Applied Biosystems 7300 real-time polymerase chain reaction (RT-PCR) system. The assay was performed with initial denaturation at 95°C for 10 min, followed by 40 PCR cycles of 95°C for 10 s and 60°C for 1 min. The average mRNA expression was normalized to the 18S ribosomal RNA expressions (Applied Biosystems).

### Western blotting

The cells were washed with PBS, and protein lysates were prepared using a mammalian cell extraction kit (BioVision, Mountain View, CA, USA). The protein concentration was determined using a Bio-Rad Protein Assay Dye Reagent Concentrate (Bio-Rad, Hercules, CA, USA) and regulated at the same level. Protein (15  $\mu$ L) from each sample was separated using 12.5% sodium dodecyl sulfate-polyacrylamide gel electrophoresis (Bio-Rad) and blotted onto a nitrocellulose membrane using transfer buffer (25 mM Tris, pH 8.8, 192 mM glycine with 20% (v/v) methanol). The membranes were blocked to any nonspecific binding in PBS with 0.1% (v/v) Tween 20 (T-PBS) containing 3% (w/v) bovine serum albumin (BSA; Sigma-Aldrich, St. Louis, MO, USA). The blots were incubated overnight at 4°C with primary antibodies. The expression of stress-activated protein kinase (SAPK)/JNK, PARP, the cleavage of caspase-8, and the cleavage of caspase-9 were detected after incubation for 3 and 72–120 h, respectively. The primary antibodies of SAPK/JNK (#9251), PARP (#9542), and the cleavage of caspase-9 (#7237) were purchased from Cell Signaling Technology (Danvers, MA, USA). The primary antibodies for detecting the cleavage of caspase-8 (#AF1650) were purchased from R&D Systems (Minneapolis, MN, USA). The antibodies for detecting SAPK/JNK, PARP, the cleavage of caspase-8, and the cleavage of caspase-9 were diluted in 0.1% T-PBS containing 3% BSA and incubated with the blots overnight at 4°C. The blots were then washed three times in T-PBS and incubated for 1 h with horseradish peroxidase (HRP)-conjugated secondary antibodies (R&D Systems, Minneapolis, MN, USA) for 1 h at room temperature. Each membrane was washed three times in 0.1% T-PBS and then developed using the Super-Signal West Pico Chemiluminescence Substrate (Thermo Fisher Scientific, Waltham, MA, USA). The chemiluminescence signal was detected using a Luminescent Image Analyzer LAS-3000 imaging system. The signals of the expression of cleaved caspase-8, p41/43, and p18 were measured at 41–43 and 18 kDa, respectively. The averaged protein expressions

were normalized to the actin expressions (BD Transduction Laboratories, Lexington, KY, USA).

### Flow cytometry

The cells were seeded at  $2.0 \times 10^6$  per 60-mm dish for 24 h prior to stimulation. After 72 h of ferrichrome treatment, the cells were then trypsinized, washed twice with PBS, and fixed in 2 mL of PBS and 4 mL of 100% ethanol. The fixed cells were incubated with 25 U/mL ribonuclease (RNase) (Wako, Osaka, Japan) at room temperature for 20 min, and propidium iodide solution was added at a final concentration of 50  $\mu$ g/mL. The cell cycle was assessed using a BD FACSCalibur (Becton, Dickinson and Company, Tokyo, Japan). The samples were analyzed by flow cytometry, and 20,000 events were obtained from each sample.

### Mass spectrometry

Ferrichrome and equimolar concentrations of iron and ferrichrome samples were prepared. The samples were diluted in methanol and injected into a Nano Frontier eLD Liquid Chromatography Mass Spectrometer (Hitachi High-Technologies, Tokyo, Japan) at 3  $\mu$ L/min. The detection mode of mass spectrometry was time of flight (TOF), and the ionization type was micro-electrospray ionization (ESI). Using the full-scan positive ion mode, the mass range was selected from 100 to 2000 Da. The drying gas flow was 1.0 L/min, and the needle/spray potential was 5800 V. The atmosphere pressure lens settings were as follows: Ex potential: 110 V, AP1 temperature: 140°C, AP2 potential: 48 V, and AP2 temperature: 140°C.

### Atomic absorption spectrometry

At 24 h before stimulation, the cells were seeded onto six-well plates at  $2.0 \times 10^5$  cells per well. After 24 h, the cells were washed with PBS and retrieved using 100  $\mu$ L of nitric acid per well. The samples were then diluted to 10% with DW. The atomic absorption of standard samples and the diluted samples was read using a Z-8100 (Hitachi High-Technologies).

### Molecular operating environment analyses

The exhaustive docking analysis of ferrichrome was performed using a Molecular Operating Environment (MOE) software program (Ryoka Systems Inc., Tokyo, Japan). The molecular information of ferrichrome was downloaded from PubChem (ID: 169636), and the ligand conformation analysis of iron-free and iron-binding ferrichrome was performed using the Amber10EHT, Born forcefield (strain energy < 100 kcal/mol). The structures of 34,495 proteins were downloaded from the Protein Data

Bank (PDB) database and optimized by the receptor conformation analysis. A docking simulation between the ligand conformation of iron-free ferrichrome and the optimized conformation of 34,495 proteins was continuously performed.

### Statistical analyses

The assay data are presented as the mean and the standard error of the mean. Student's *t* test, a one-way analysis of variance, and Bonferroni correction were used for the statistical analyses. *p* values <0.05 were considered to indicate statistical significance using Student's *t* test and the one-way analysis of variance. When *p* values were less than 0.05, Bonferroni correction was used to detect significant differences between groups. In such cases, *p* values <0.0083 and 0.017 were considered to indicate statistical significance of differences among four and three samples, respectively.

## Results

### *Ferrichrome-suppressed gastric cancer cell progression*

To clarify the tumor-suppressive effects of ferrichrome in gastric cancer cells, SRB and MTT assays were performed. These assays revealed the growth suppression effects of ferrichrome in all gastric cancer cells after 72–120 h treatment. Ferrichrome exerted stronger tumor-suppressive effects in MKN-7 and MKN-45 than MKN-74 and NUGC-4. The growth-suppressive effects were correlated with the concentration of ferrichrome (Figure 1). MKN-45 cells were injected into the backs of nude mice to build xenograft models. Ferrichrome was intraperitoneally injected every day, and the tumor sizes were measured. The tumor size of the ferrichrome-treated group was significantly smaller than that in the control group (Figure 2(a) and (b)). These findings indicated that ferrichrome exerted growth-suppressive effects in gastric cancer cells. After treatment of the xenograft models, blood samples were collected from the inferior vena cava. The level of hemoglobin and mean corpuscular volume (MCV) were examined because ferrichrome is an iron chelator ferrichrome. There was no marked difference in the levels of hemoglobin and MCV between the control group and the ferrichrome-treated group (Figure 2(c) and (d)).

### *The ferrichrome induced apoptotic pathway*

Our recent study revealed that ferrichrome induced apoptosis mediated by the activation of the JNK-DDIT3 pathway in colorectal cancer cells,<sup>10</sup> and the expression of apoptosis-associated molecules was assessed in gastric cancer cells. The expression levels of cleaved PARP and cleaved

caspase-9 were significantly induced by the administration of 100 µg/mL ferrichrome. Even 1 µg/mL ferrichrome induced the expression of cleaved PARP in MKN-45 and MKN-74 cells. Although the cleavage of caspase-8 was not detected in MKN-45 cells, it was detected in the other gastric cancer cells (Figure 3(a)–(d)). Next, JNK-DDIT3-mediated apoptotic signaling pathway was assessed under treatment with ferrichrome in gastric cancer cells. A western blotting analysis showed that the phosphorylation of JNK was upregulated in ferrichrome-treated cells compared to control cells (Figure 3(e)). A real-time polymerase chain reaction (RT-PCR) analysis indicated that the mRNA levels of DDIT3 significantly increased in MKN-45 cells by the ferrichrome treatment (Figure 3(f)). The cell cycle was then assessed by flow cytometry. Ferrichrome treatment was found to change the cancer cell cycle and increase the sub-G1 peak in MKN-74 cells, but not in MKN-7, MKN-45, or NUGC-4 cells (Figure 3(g)–(j)). These findings indicated that ferrichrome inhibited the cell cycle and upregulated the cell death pathway, including the JNK-DDIT3 pathway, in gastric cancer cells.

### *Iron-chelated ferrichrome did not inhibit the cancer cell growth*

Ferrichrome reportedly has the ability to chelate metal agents, including iron.<sup>11–13</sup> A mass spectrometry analysis of ferrichrome revealed that the *m/z* of iron-free ferrichrome was shifted completely by adding equal molecular concentrations of FeCl<sub>3</sub>, suggesting that ferrichrome chelated iron at a 1:1 molecular ratio (Figure 4(a) and (b)). To elucidate the tumor-suppressive effects of iron-chelated ferrichrome, an SRB assay and MTT assay were performed. These assays indicated that the tumor-suppressive effects of ferrichrome were canceled on iron chelation in gastric cancer cells (Figure 4(c)–(f)). An RT-PCR of DDIT3 mRNA was performed in gastric cancer cells, with results showing that the induction of DDIT3 mRNA by 1 µg/mL ferrichrome was diminished by iron chelation in MKN-7 and MKN-45 (Figure 4(g) and (h)). There was no marked change in the expression of DDIT3 mRNA in examinations of 100 µg/mL ferrichrome in MKN-74 or NUGC-4, respectively, (Figure 4(i) and (j)).

We further assessed whether or not ferrichrome depleted intracellular iron in gastric cancer cells. An atomic absorption spectrometry analysis indicated that the intracellular iron contents were reduced by iron-free ferrichrome treatment. However, the reduction in intercellular iron did not significantly differ between 1 and 100 µg/mL of ferrichrome treatment in these cell lines (Figure 4(k)), and the grade of growth inhibition by 1 µg/mL ferrichrome was much lower than that by 100 µg/mL of ferrichrome in MKN-7 and MKN-45 (Figure 1(a) and (b)). In addition, although 1 µg/mL of ferrichrome equally depleted intracellular iron compared with 100 µg/mL in MKN-74 and

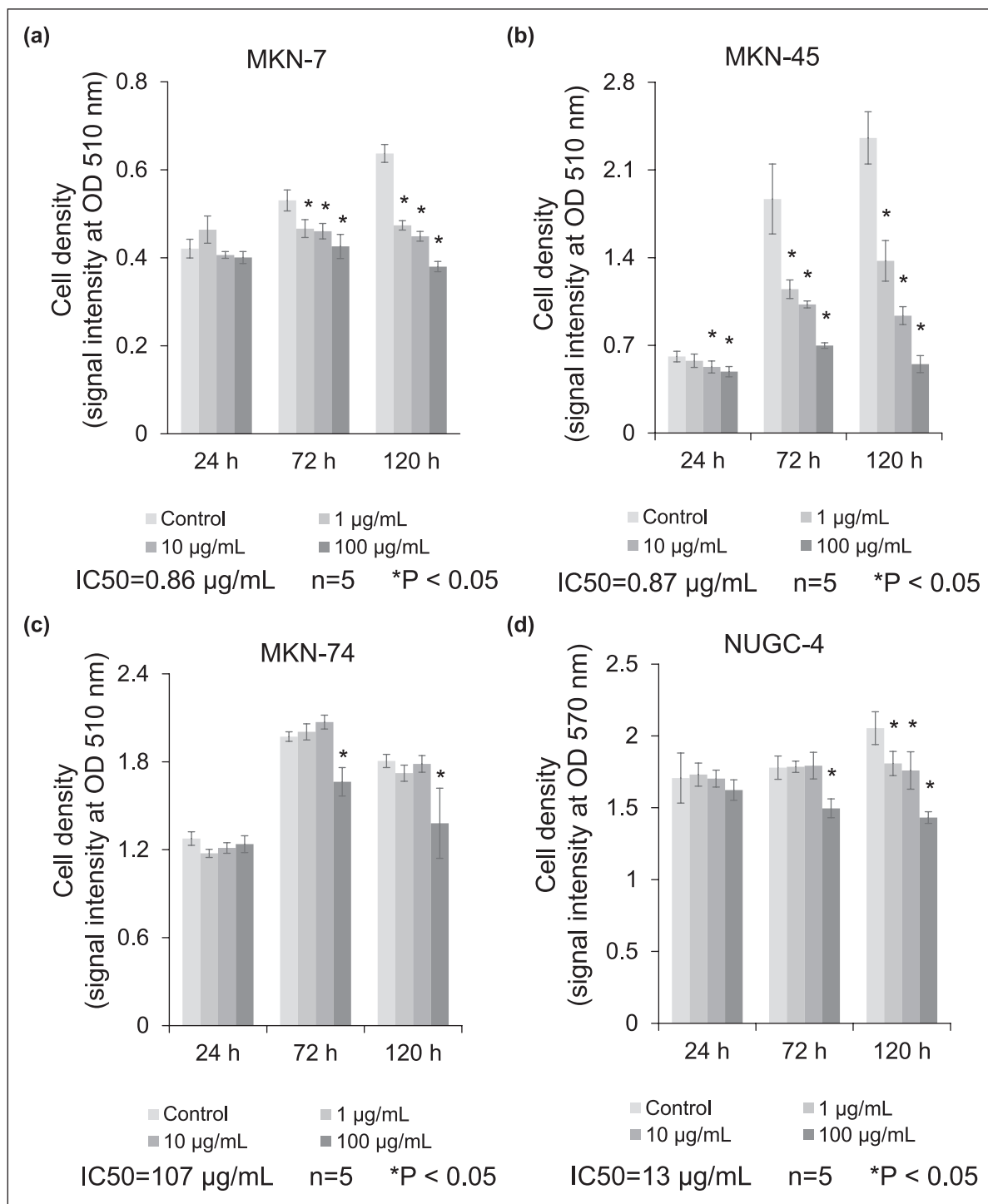


**Figure 1.** Ferrichrome exerted tumor-suppressive effects on gastric cancer cells. Ferrichrome inhibited cancer cell progression dose dependently in (a) MKN-7 and (b) MKN-45. Only a high dose of ferrichrome exerted tumor-suppressive effects in (c) MKN-74 and (d) NUGC-4. The half maximal inhibitory concentration (IC<sub>50</sub>) at 72 h and the sample size (n) were indicated. \*p < 0.05 by Student's t test. All data are represented as the mean ± SE (see also Figure S1).

NUGC-4 cells (Figure 4(k)), anticancer effects were only detected on treatment with ≥100 µg/mL of ferrichrome (Figure 1(c) and (d)). These results indicated that the reduction in the intracellular iron concentration did not correlate with the anticancer effects of ferrichrome.

#### *Ferrichrome forms stable conformations with various molecules*

As shown above, the tumor-suppressive effects of ferrichrome did not appear to be associated with a decrease in

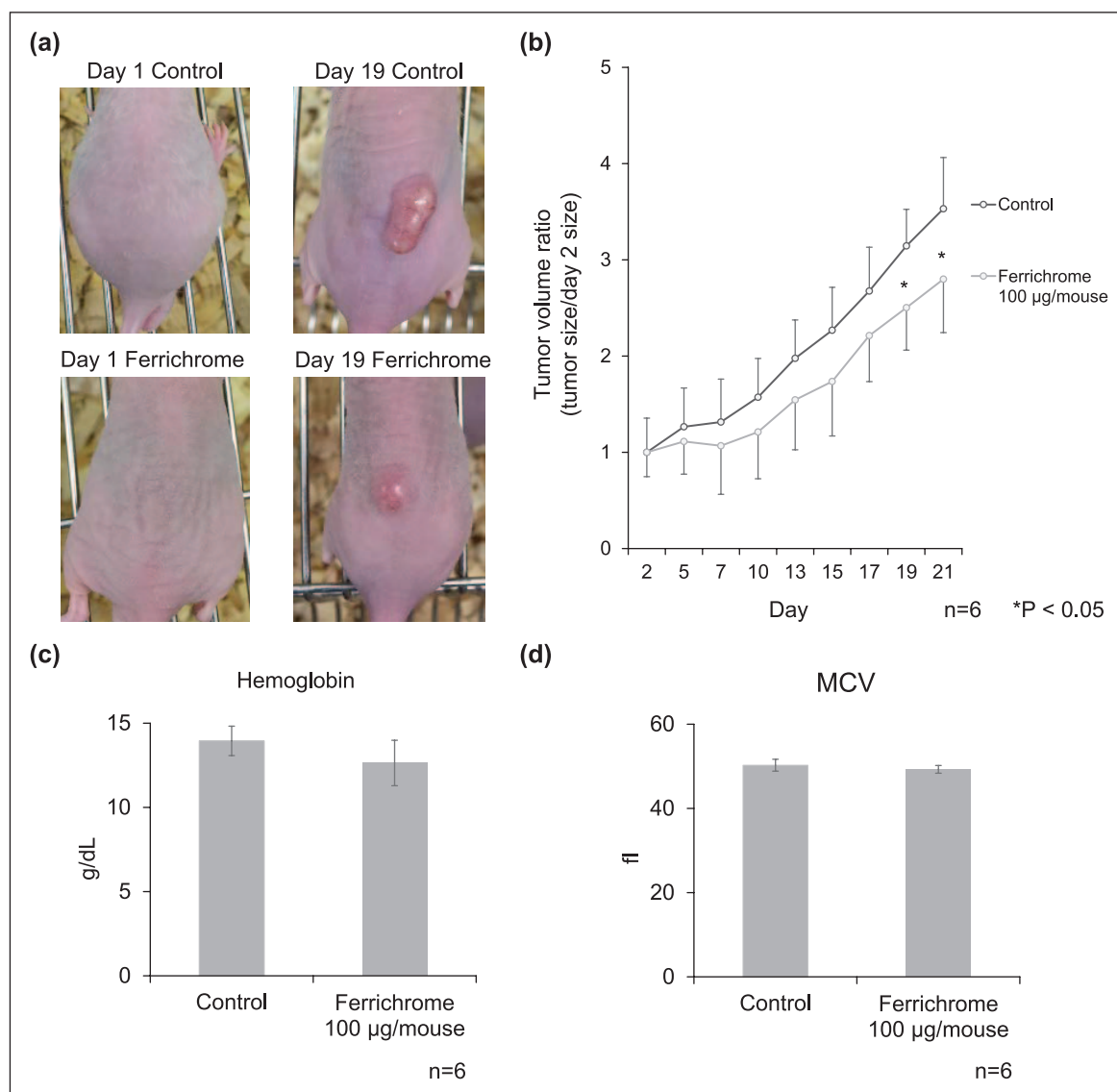


**Figure 2.** Ferrichrome exerted tumor-suppressive effects in xenograft mice (related to Figure 1). Distilled water and 100 µg ferrichrome were administered by intraperitoneal injection to the control group and treatment group, respectively. (a and b) Ferrichrome suppressed the tumor size in the treatment group to a greater degree than in the control group. The administration of ferrichrome did not change the (c) hemoglobin or (d) MCV levels in mice. The sample size (n) is indicated. \* $p < 0.05$  by Student's t test. All data are represented as the mean  $\pm$  SD.

the iron concentration of cancer cells. An exhaustive docking simulation was performed to identify the target molecules of ferrichrome in gastric cancer cells. The ligand conformation analysis indicated that iron-free ferrichrome could construct 9980 conformations under 100 kcal/mol of strain energy. A receptor conformation analysis was continuously performed for optimization of the structures of 34,495 proteins downloaded from the PDB. A docking simulation was then performed between 9980 conformations of iron-free ferrichrome and the optimized structure of 34,495 proteins. The candidate human molecules capable of forming stable conformations with iron-free ferrichrome are listed in Table 1. The conformation of

iron-binding ferrichrome was fixed in a single structure, and only one docking partner among bacterial molecules (and no mammalian molecules) was found to be able to form a conformation under 100 kcal/mol of strain energy. These findings indicated that iron-free ferrichrome has greater potential to bind to various molecules, likely cancer cell-derived molecules, than the iron-binding form.

## Discussion

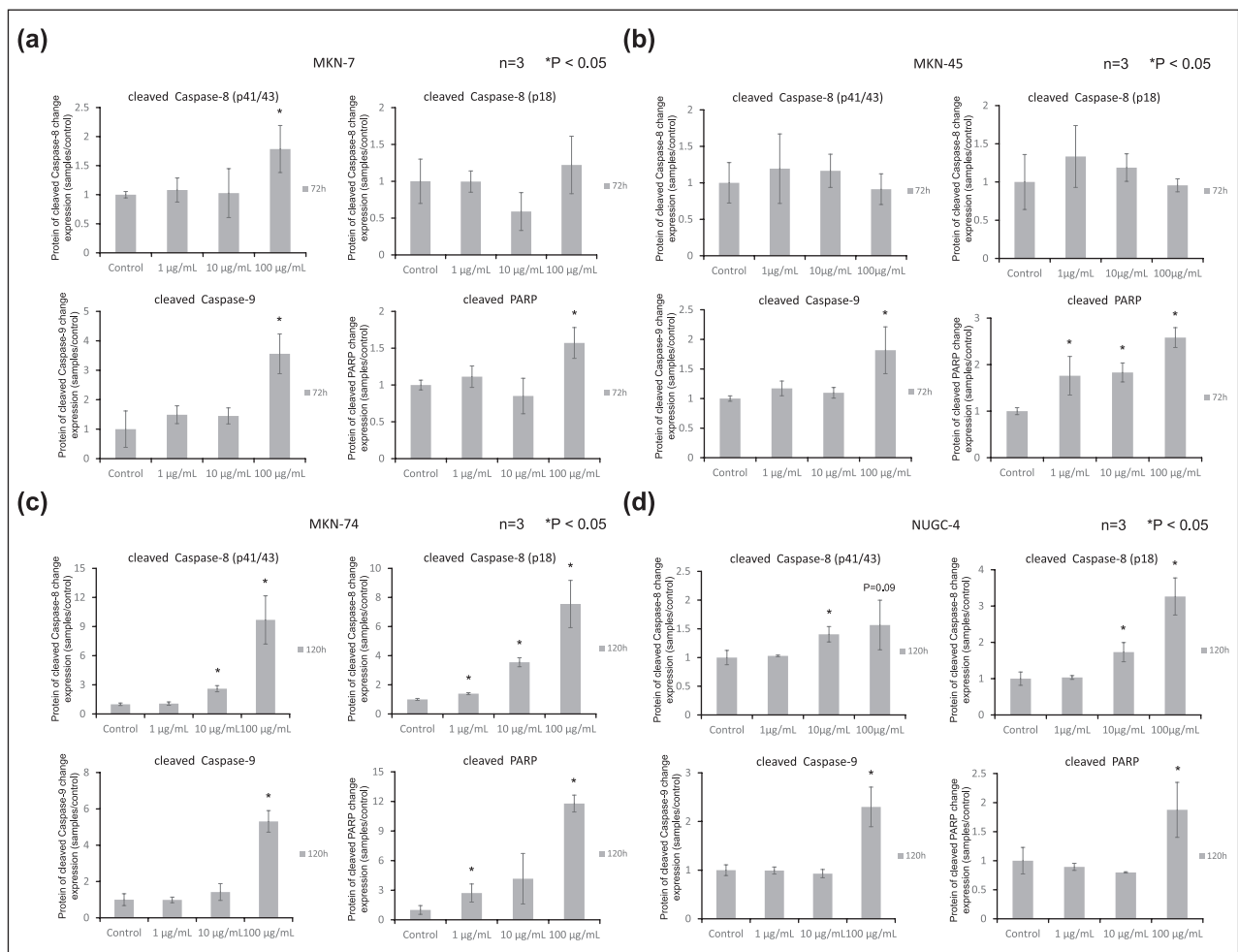
We recently identified the tumor-suppressive molecule ferrichrome from conditioned media of *L. casei* and showed that it induced apoptosis in colorectal cancer cells.<sup>10</sup>

However, the tumor-suppressive effects on other gastrointestinal cancer cells and details of the mechanisms remained unclear. This study revealed for the first time that ferrichrome derived from *L. casei* has strong tumor-suppressive effects on gastric cancer cells, probably by inducing JNK-DDIT3-mediated apoptosis. Of note, the tumor-suppressive effects of ferrichrome were mediated through its iron-binding site, although the iron concentration was not associated with the tumor-suppressive effects, suggesting that ferrichrome targets other molecules in gastric cancer cells.

SRB and MTT assays showed that ferrichrome exerted dose-dependent tumor-suppressive effects on gastric cancer cells (Figure 1). Ferrichrome is a siderophore, which is an iron-chelating agent derived from bacteria.<sup>11–13</sup> Previous reports have shown that iron chelators exert their anticancer effects by depleting intracellular iron.<sup>20–22</sup> To determine whether or not an iron-binding site of ferrichrome is necessary for it to exert its tumor-suppressive effects, complete iron-bound ferrichrome was used for SRB and MTT assays. These assays showed that the tumor-suppressive

effects of ferrichrome were negated by iron binding. We therefore speculated that the tumor-suppressive effects of ferrichrome were associated with a decrease in the iron concentration in cancer cells. However, the concentration of intracellular iron was not correlated with the growth inhibition by ferrichrome (Figure 4(k)), indicating that a decrease in the intracellular iron concentration was not essential for ferrichrome to exert its tumor-suppressive effects. Thus, ferrichrome operates via a novel anticancer mechanism by interacting with the cell components, regardless of the intracellular concentration of iron, to induce apoptosis in gastric cancer cells.

Subsequently, the docking molecules which bound iron-free or iron-binding ferrichrome were analyzed using an MOE software program. The analysis identified several candidate human molecules capable of binding to iron-free ferrichrome (Table 1). Conversely, iron-chelated ferrichrome was unable to bind to any human molecules, suggesting that the iron-free structure of ferrichrome can capture unknown molecules in cancer cells through the iron-binding site. Previous reports indicated the relevance



(continued)

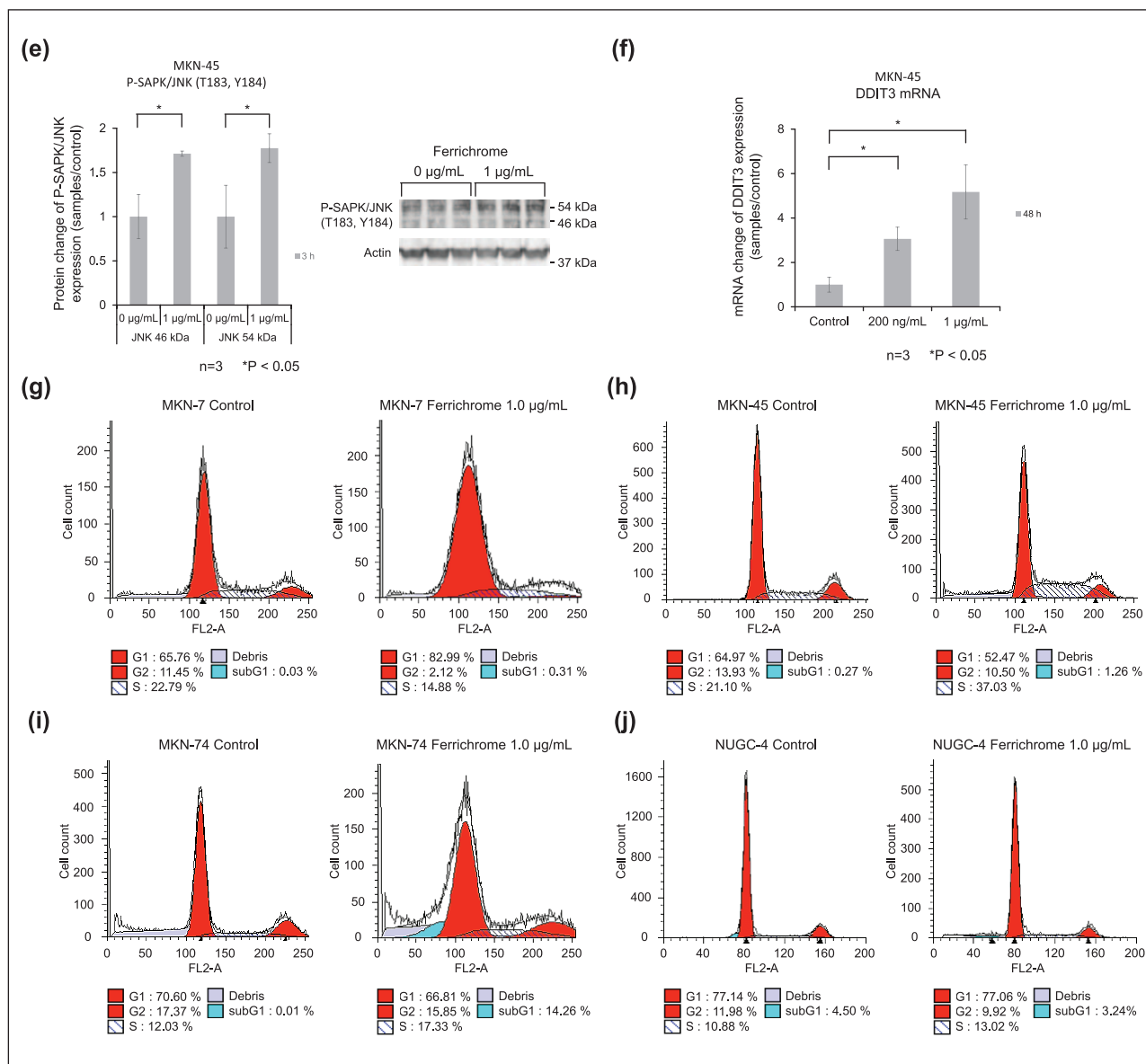


**Figure 3.** Ferrichrome induced apoptosis through the JNK-DDIT3-mediated pathway in gastric cancer cells. (a–d) The expression of cleaved PARP, cleaved caspase-8, and cleaved caspase-9 in gastric cancer cells and (e) the phosphorylation of SAPK/JNK in MKN-45 were assessed by western blotting. The expression levels of cleaved PARP and cleaved caspase-9 were significantly induced by the administration of 100  $\mu\text{g/mL}$  ferrichrome. Even 1  $\mu\text{g/mL}$  ferrichrome induced the expression of cleaved PARP in MKN-45 and MKN-74 cells. (a–d) Although the cleavage of caspase-8 was not detected in MKN-45 cells, it was detected in other gastric cancer cells. (f) DDIT3 mRNA was dose dependently induced by ferrichrome treatment in MKN-45 cells. The cell cycle was assessed by flow cytometry in gastric cancer cells; the fluorescence strength was measured by the FL2-A channel, which was captured at a wavelength of  $585 \pm 21$  nm. Ferrichrome treatment was found to change the cancer cell cycle and increase sub-G1 peak in MKN-74 cells, but not in (g–j) MKN-7, MKN-45, or NUGC-4 cells. The sample size (n) is indicated. \* $p < 0.05$  by Student's t test. All data are represented as the mean  $\pm$  SE.

of the JNK-DDIT3 pathway and predicted that three molecules, threonine-tRNA ligase, Son of sevenless homolog 1 (SOS1), and methylthioribulose-1-phosphate dehydratase (APIP), would interact with ferrichrome. Multi-tRNA synthetases such as threonine-tRNA ligase inhibit the activation of JNK,<sup>23</sup> and the inhibition of threonine-tRNA ligase induces the DDIT3-apoptotic pathway.<sup>24</sup>

Thus, we suspect that ferrichrome may inhibit the anti-apoptotic function of threonine-tRNA ligase through the activation of the JNK-DDIT3-mediated pathway in gastric cancer cells. The SOS family is an important Ras signaling regulator. SOS1 inhibits apoptosis through the activation of the HRAS-PI3K cascade.<sup>25</sup> APIP functions in the methionine salvage pathway and inhibits the

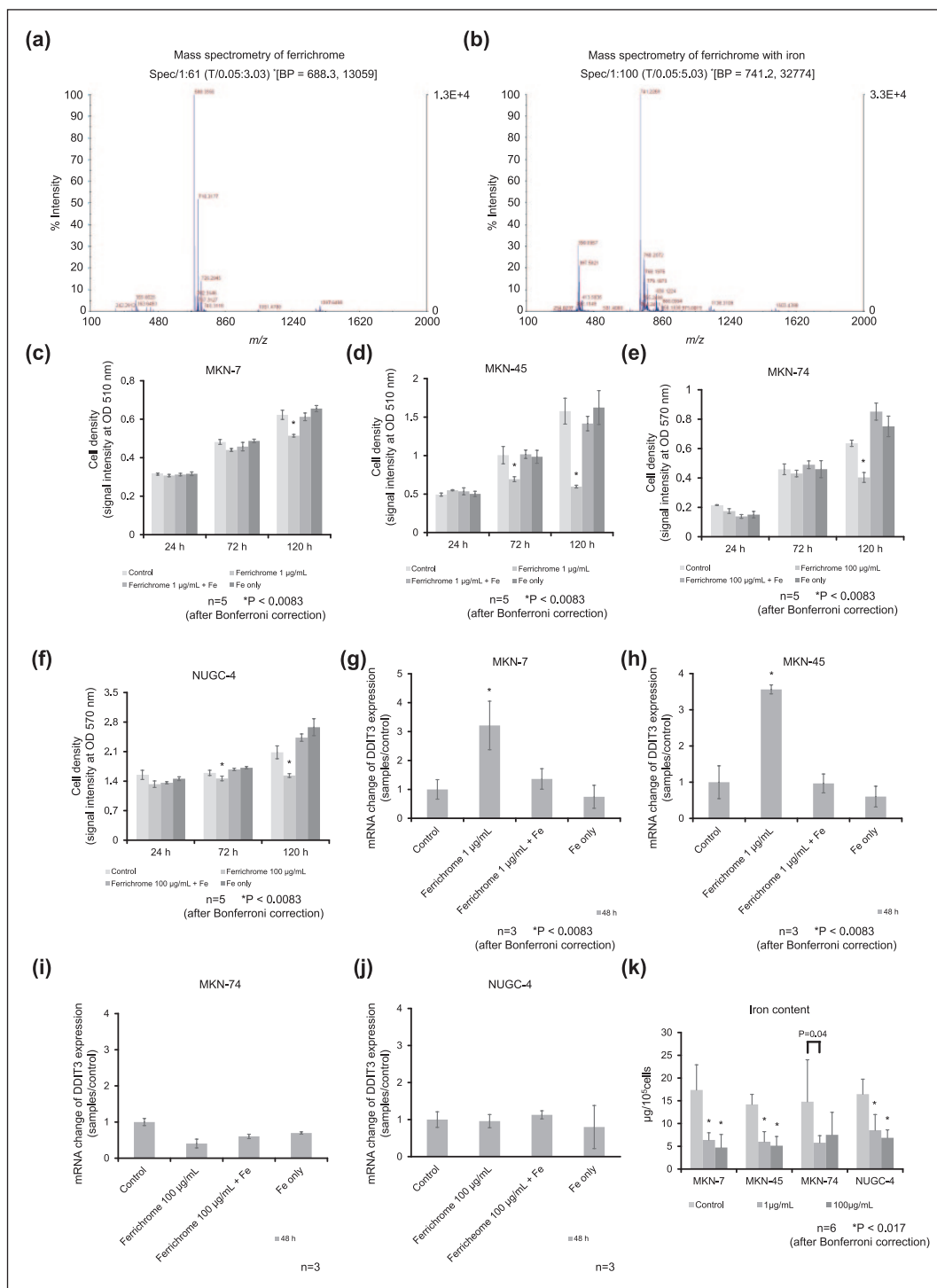


**Figure 4.** Ferrichrome-chelated iron and lost its tumor-suppressive effects, but the intracellular iron concentration was not correlated with cell viability. (a) Mass spectrometry analyses revealed the  $m/z$  ratio of iron-free ferrichrome. (b) The  $m/z$  ratio of iron-free ferrichrome was completely shifted by iron chelation. The SRB and MTT assays showed that the tumor-suppressive effects of 1 and 100 µg/mL ferrichrome were inhibited by equimolar iron chelation in (c) MKN-7, (d) MKN-45, (e) MKN-74, and (f) NUGC-4. The induction of DDIT3 by 1 and 100 µg/mL ferrichrome was diminished by iron chelation in (g) MKN-7 and (h) MKN-45, (i) MKN-74 and (j) NUGC-4. (k) Atomic absorption spectrometry revealed that ferrichrome depleted intracellular iron independent on the drug concentration in gastric cancer cells. The sample size ( $n$ ) is indicated. The one-way analysis of variance showed significant differences in the means between each group in Figures 4(c)–(h) (\* $p$  < 0.0083 after Bonferroni correction) and in the means between the control and each ferrichrome treatment group in Figure 4(k) (\* $p$  < 0.017 by Bonferroni correction). All data are represented as the mean  $\pm$  SE.

**Table 1.** Iron-free ferrichrome can form stable conformations with various mammalian molecules.

No.	Candidate molecules that can bind to iron-free ferrichrome	No.	Candidate molecules that can bind to iron-free ferrichrome	No.	Candidate molecules that can bind to iron-free ferrichrome
1	cAMP-specific 3',5'-cyclic phosphodiesterase 4A	11	Interferon-induced protein with tetratricopeptide repeats 5	21	Tyrosyl-tRNA synthetase
2	Phosphatidylcholine transfer protein	12	Inosine monophosphate dehydrogenase I	22	Poly(ADP-ribose) polymerase 3
3	Cystathionine beta-synthase	13	SUMO-activating enzyme subunit I	23	DNA repair protein REV1
4	DNA mismatch repair protein Msh2	14	Threonine—tRNA ligase, cytoplasmic	24	S-phase kinase-associated protein 1A
5	P2Y purinoceptor 1, Rubredoxin, P2Y purinoceptor 1	15	CCA tRNA nucleotidyltransferase I, mitochondrial	25	Cyclin-dependent kinase 9
6	Histone-binding protein RBBP7 (pRB-associated proteins p46)	16	Ceruloplasmin	26	U3 small nucleolar RNA-interacting protein 2
7	Poly(ADP-ribose) polymerase family, member 11	17	Inositol hexakisphosphate and diphosphoinositol-pentakisphosphate kinase 2	27	Chimera protein of human 5-hydroxytryptamine receptor 1B and <i>Escherichia coli</i> -soluble cytochrome b562
8	Histone-lysine N-methyltransferase 2D	18	RNA-specific adenosine deaminase B1, isoform DRADA2a	28	Methylthioribulose-1-phosphate dehydratase
9	E3 ubiquitin-protein ligase MIB1	19	Cell division protein kinase 7	29	Eukaryotic translation initiation factor 4E type 2
10	Son of sevenless homolog 1	20	Sialidase 2	30	5'-AMP-activated protein kinase catalytic subunit alpha-1

RBBP: retinoblastoma-binding protein; MIB: mind bomb; SUMO: small ubiquitin-related modifier; DRADA: double-stranded RNA-specific adenosine deaminase; tRNA: transfer RNA; ADP: adenosine diphosphate; AMP: adenosine monophosphate.

caspase-9-mediated apoptotic pathway.<sup>26</sup> We hypothesize that ferrichrome binds with threonine-tRNA ligase, SOS1, and/or AIP and inhibits their functions, resulting in the induction of apoptosis in gastric cancer cells. Further analyses to determine the molecules captured by iron-free ferrichrome, particularly threonine-tRNA ligase, SOS1, and AIP may be useful for identifying novel targets of cancer treatments.

Our previous report proposed that ferrichrome induced the expression of apoptotic transcriptional factor DDIT3 in colon cancer cells.<sup>10</sup> Similarly, this study revealed that ferrichrome induced DDIT3 in MKN-7 and MKN-45, suggesting that DDIT3 is a key factor for inducing apoptosis in gastric cancer cells. However, DDIT3 was not induced in MKN-74 or NUGC-4 by ferrichrome treatment. Our SRB assay showed that the growth of these two cell lines was suppressed by only high-concentration (100 µg/mL) ferrichrome, suggesting that high-concentration ferrichrome exerts its tumor-suppressive effects via an alternative mechanism.

Western blotting showed that the expression of cleaved caspase-8, caspase-9, and PARP was induced in gastric cancer cells. Flow cytometry showed that the sub-G1 peak was increased in MKN-74 cells and that G1 arrest occurred in MKN-7 cells. The results indicated that the anti-tumor effects of ferrichrome not only occurred via the apoptotic

pathway but also involved changes in the cell cycles. An SRB assay showed that only 100 µg/mL ferrichrome exerted the tumor-suppressive effects in MKN-74 cells. These results suggested that proliferative potential of the cells was greater than the tumor-suppressive effects of 1–10 µg/mL ferrichrome. In NUGC-4 cells, 10 and 100 µg/mL ferrichrome induced the expression of cleaved caspase-8, cleaved-9, and PARP, and there was no change in the flow cytometry peak. Thus, high-concentration ferrichrome could induce apoptotic effects in NUGC-4 cells. In MKN-45 cells, the expression levels of cleaved caspase-9 and PARP were increased, but there was no significant change in the cleaved caspase-8 and sub-G1 peaks. These data suggest that ferrichrome has the potential to upregulate not only the JNK-DDIT3 apoptotic pathway but also other tumor-suppressive pathways. Necroptosis is a programmed cell death mechanism that is characterized by various morphological characteristics, including the swelling of the cells and the absence of nuclear condensation and hypoploid particles.<sup>27</sup> The caspase-8 activity is a key factor in the induction of apoptosis, and a lack of caspase-8 activity leads to necroptosis in this pathway.<sup>28,29</sup> Further studies should be performed to determine whether ferrichrome is associated with other cell death pathways in MKN-45 cells.

Bacteria-derived ferrichrome is thought to act as a metal chelator, and while it may also exert other effects,

none have yet been identified. This study and our previous investigation<sup>10</sup> suggested that ferrichrome is a multifunction molecule that acts as a mediator for host-microbe interactions, including the mediation of probiotic tumor-suppressive effects on cancer cells. Ferrichrome and other bacteria-derived siderophores may mediate host-microbe interactions in some manner. Identifying the functions of these siderophores will clarify novel mechanisms of host-microbe interactions and may aid in the development of new drugs for the treatment of many human disorders.

### Acknowledgements

The authors thank Akemi Kita and Kotoe Shibusa for their technical assistance. M.I., M.F., and H.K. contributed equally to this study and provided major input on the conceptual development of the studies, wrote the manuscript, and supervised all investigations. M.I. and H.K. performed the biochemical experiments. H.T., N.U., S.K., K.M., J.S., K.I., and T.O. helped to design studies, interpret the data, and prepare/review the manuscript. All the authors read and approved the final manuscript.

### Declaration of conflicting interests

The author(s) declared no potential conflicts of interest with respect to the research, authorship, and/or publication of this article.

### Funding

The author(s) disclosed receipt of the following financial support for the research, authorship, and/or publication of this article: This paper was supported by Grants-in-Aid for Scientific Research, no. 26460956 (M.F.), 16H06607 (H.K.) and 25460923 (K.M.) and Intractable Disease Health and Labour Sciences Research Grants from the Ministry of Health, Labour and Welfare.

### References

1. Food and Agriculture Organization and WHO. *Guidelines for the evaluation of probiotics in food*. London, ON, Canada: WHO, 2002.
2. Isolauri E and Salminen S. Probiotics: use in allergic disorders: a Nutrition, Allergy, Mucosal Immunology, and Intestinal Microbiota (NAMI) Research Group report. *J Clin Gastroenterol* 2008; 42(Suppl 2): S91–S96.
3. Kalliomäki M, Salminen S, Arvilommi H, et al. Probiotics in primary prevention of atopic disease: a randomised placebo-controlled trial. *Lancet* 2001; 357: 1076–1079.
4. Rowland IR, Rumney CJ, Coutts JT, et al. Effect of *Bifidobacterium longum* and inulin on gut bacterial metabolism and carcinogen-induced aberrant crypt foci in rats. *Carcinogenesis* 1998; 19: 281–285.
5. Fujiya M, Musch MW, Nakagawa Y, et al. The *Bacillus subtilis* quorum-sensing molecule CSF contributes to intestinal homeostasis via OCTN2, a host cell membrane transporter. *Cell Host Microbe* 2007; 1: 299–308.
6. Kahima S, Fujiya M, Konishi H, et al. Polyphosphate, an active molecule derived from probiotic *Lactobacillus brevis*, improves the fibrosis in murine colitis. *Transl Res* 2015; 166: 163–175.
7. Segawa S, Fujiya M, Konishi H, et al. Probiotic-derived polyphosphate enhances the epithelial barrier function and maintains intestinal homeostasis through integrin-p38 MAPK pathway. *PLoS ONE* 2011; 6: e23278.
8. Tanaka K, Fujiya M, Konishi H, et al. Probiotic-derived polyphosphate improves the intestinal barrier function through the caveolin-dependent endocytic pathway. *Biochem Biophys Res Commun* 2015; 467: 541–548.
9. Sakatani A, Fujiya M, Ueno N, et al. Polyphosphate derived from *Lactobacillus brevis* inhibits colon cancer progression through induction of cell apoptosis. *Anticancer Res* 2016; 36: 591–598.
10. Konishi H, Fujiya M, Tanaka H, et al. Probiotic-derived ferrichrome inhibits colon cancer progression via JNK-mediated apoptosis. *Nat Commun* 2016; 7: 12365.
11. Gueriot ML. Microbial iron transport. *Annu Rev Microbiol* 1994; 48: 743–772.
12. Poole K and McKay GA. Iron acquisition and its control in *Pseudomonas aeruginosa*: many roads lead to Rome. *Front Biosci* 2003; 8: d661–d686.
13. Saha R, Saha N, Donofrio RS, et al. Microbial siderophores: a mini review. *J Basic Microbiol* 2013; 53: 303–317.
14. Tabas I and Ron D. Integrating the mechanisms of apoptosis induced by endoplasmic reticulum stress. *Nat Cell Biol* 2011; 13: 184–190.
15. Li G, Mongillo M, Chin KT, et al. Role of ERO1-alpha-mediated stimulation of inositol 1,4,5-triphosphate receptor activity in endoplasmic reticulum stress-induced apoptosis. *J Cell Biol* 2009; 186: 783–792.
16. Timmins JM, Ozcan L, Seimon TA, et al. Calcium/calmodulin-dependent protein kinase II links ER stress with Fas and mitochondrial apoptosis pathways. *Clin Invest* 2009; 119: 2925–2941.
17. Li G, Scull C, Ozcan L, et al. NADPH oxidase links endoplasmic reticulum stress, oxidative stress, and PKR activation to induce apoptosis. *J Cell Biol* 2010; 191: 1113–1125.
18. Kaufmann T, Strasser A and Jost PJ. Fas death receptor signaling: roles of Bid and XIAP. *Cell Death Differ* 2012; 19: 42–50.
19. Vichai V and Kirtikara K. Sulforhodamine B colorimetric assay for cytotoxicity screening. *Nat Protoc* 2006; 1: 1112–1116.
20. Buss JL, Torti FM and Torti SV. The role of iron chelation in cancer therapy. *Curr Med Chem* 2003; 10: 1021–1034.
21. Hann HW, Stahlhut MW, Rubin R, et al. Antitumor effect of deferoxamine on human hepatocellular carcinoma growing in athymic nude mice. *Cancer* 1992; 70: 2051–2056.
22. Le NT and Richardson DR. The role of iron in cell cycle progression and the proliferation of neoplastic cells. *Biochim Biophys Acta* 2002; 1603: 31–46.
23. Ko YG, Kim EY, Kim T, et al. Glutamine-dependent antiapoptotic interaction of human glutaminyl-tRNA synthetase with apoptosis signal-regulating kinase 1. *J Biol Chem* 2001; 276: 6030–6036.
24. Habibi D, Ogloff N, Jalili RB, et al. Borrelidin, a small molecule nitrile-containing macrolide inhibitor of threonyl-tRNA synthetase, is a potent inducer of apoptosis in acute lymphoblastic leukemia. *Invest New Drugs* 2012; 30: 1361–1370.
25. Liu K, Jiang T, Ouyang Y, et al. Nuclear EGFR impairs ASPP2-p53 complex-induced apoptosis by inducing SOS1 expression in hepatocellular carcinoma. *Oncotarget* 2015; 6: 16507–16516.

26. Cho DH, Hong YM, Lee HJ, et al. Induced inhibition of ischemic/hypoxic injury by APIP, a novel Apaf-1-interacting protein. *J Biol Chem* 2004; 279: 39942–39950.
27. Vercammen D, Brouckaert G, Denecker G, et al. Dual signaling of the Fas receptor: initiation of both apoptotic and necrotic cell death pathways. *J Exp Med* 1998; 188: 919–930.
28. Holler N, Zaru R, Micheau O, et al. Fas triggers an alternative, caspase-8-independent cell death pathway using the kinase RIP as effector molecule. *Nat Immunol* 2000; 1: 489–495.
29. Vandenabeele P, Galluzzi L, Vanden Berghe T, et al. Molecular mechanisms of necroptosis: an ordered cellular explosion. *Nat Rev Mol Cell Biol* 2010; 11: 700–714.